Supplemental Material: Guidelines for accurate and efficient calculations of mobilities in two-dimensional materials

Jiaqi Zhou,[1,*] Samuel Poncé,[1,2,3,†] and Jean-Christophe Charlier[1,‡]

[1]*Institute of Condensed Matter and Nanosciences (IMCN), Université catholique de Louvain (UCLouvain), 1348 Louvain-la-Neuve, Belgium*
[2]*European Theoretical Spectroscopy Facility*
[3]*WEL Research Institute, Avenue Pasteur 6, 1300 Wavre, Belgium*

(Dated: April 12, 2024)

S1. ATOMIC STRUCTURE

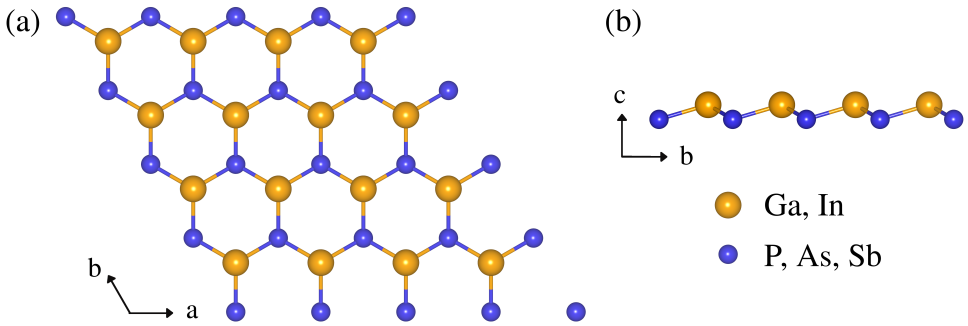


FIG. S1. Atomic structure of III-V monolayer in the honeycomb structure with a low-buckling height. (a) Top view. (b) Side view.

TABLE S1. Fully relaxed lattice constants a and buckling heights h of 2D materials by the stringent fully relativistic pseudopotential.

2DM	GaP	InP	GaAs	InAs	GaSb	InSb
a (Å)	3.90	4.22	4.05	4.36	4.38	4.68
h (Å)	0.39	0.50	0.58	0.66	0.70	0.76

* jiaqi.zhou@uclouvain.be
† samuel.ponce@uclouvain.be
‡ jean-christophe.charlier@uclouvain.be

S2. ORBITALS IN PSEUDOPOTENTIALS AND DEFORMATION POTENTIALS OF In As

TABLE S2. Orbitals included in the valence, standard, and stringent pseudopotentials of elements involved in this work.

Element	valencePP	standardPP	stringentPP
Ga	$4s^2 4p^1$	$3d^{10} 4s^2 4p^1$	$3s^2 3p^6 3d^{10} 4s^2 4p^1$
In	$5s^2 5p^1$	$4d^{10} 5s^2 5p^1$	$4s^2 4p^6 4d^{10} 5s^2 5p^1$
P	$3s^2 3p^3$	$3s^2 3p^3$	$3s^2 3p^3$
As	$4s^2 4p^3$	$3d^{10} 4s^2 4p^3$	$3s^2 3p^6 3d^{10} 4s^2 4p^3$
Sb	$5s^2 5p^3$	$4d^{10} 5s^2 5p^3$	$4s^2 4p^6 4d^{10} 5s^2 5p^3$

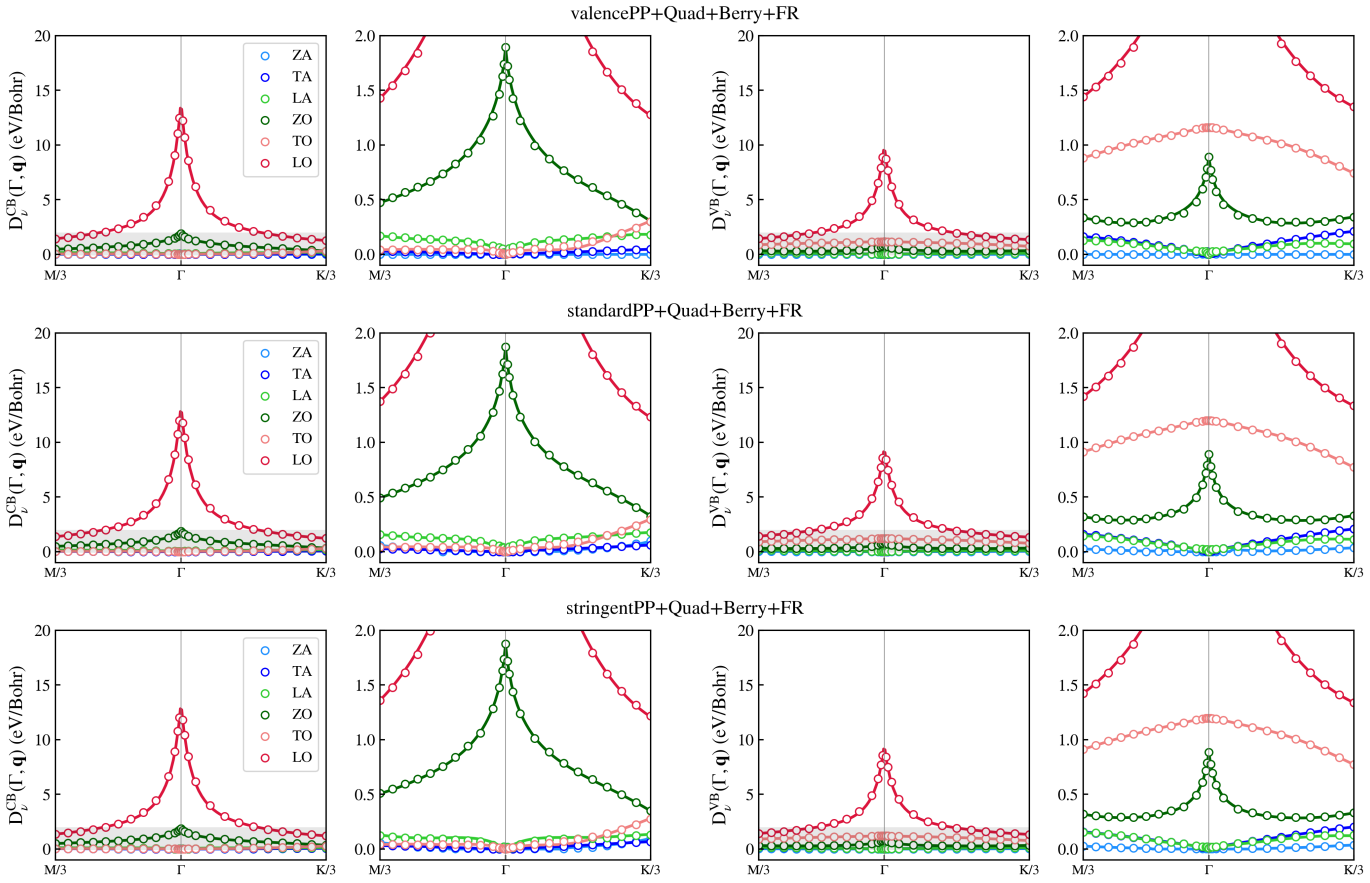


FIG. S2. Comparison between the deformation potential from the direct DFPT calculations (dots) and that from the Wannier interpolation (lines). The left two columns show the conduction bands and zoomed-in shadowed region, the right two columns show the valence bands and zoomed-in shadowed region. The valence, standard, and stringent pseudopotentials are respectively employed to calculate the deformation potential of InAs monolayer.

S3. GaP

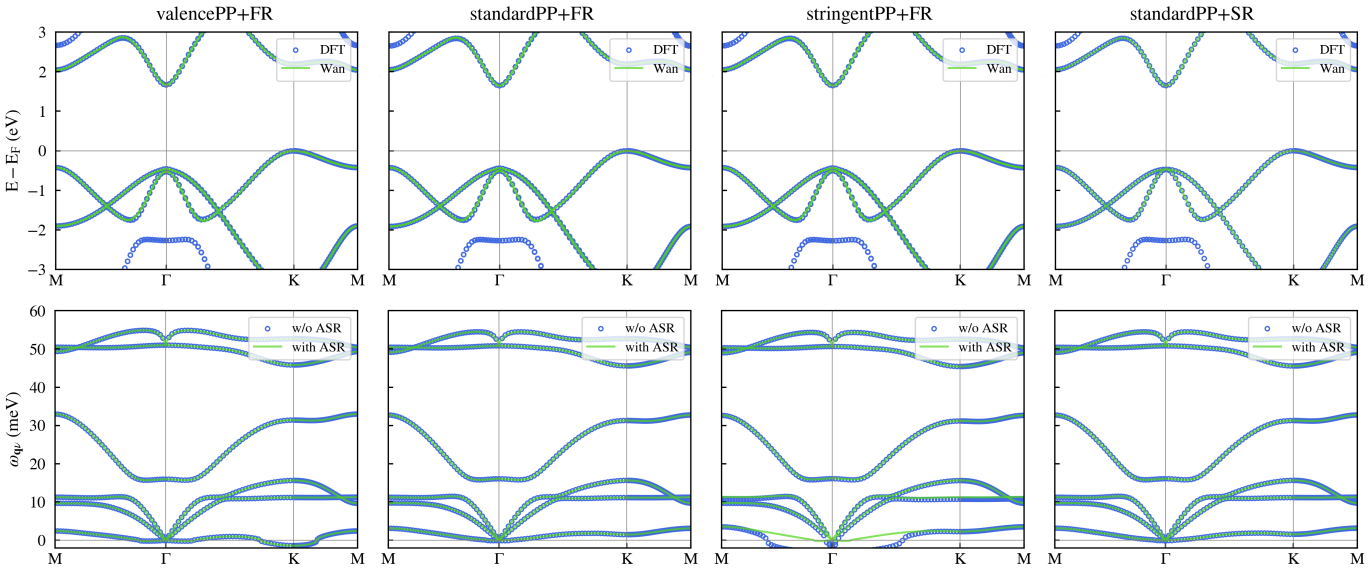


FIG. S3. Electronic bands (the first row) and phonon dispersions (the second row) calculated by different pseudopotentials. The effects of acoustic sum rule (ASR) are shown in phonon dispersions.

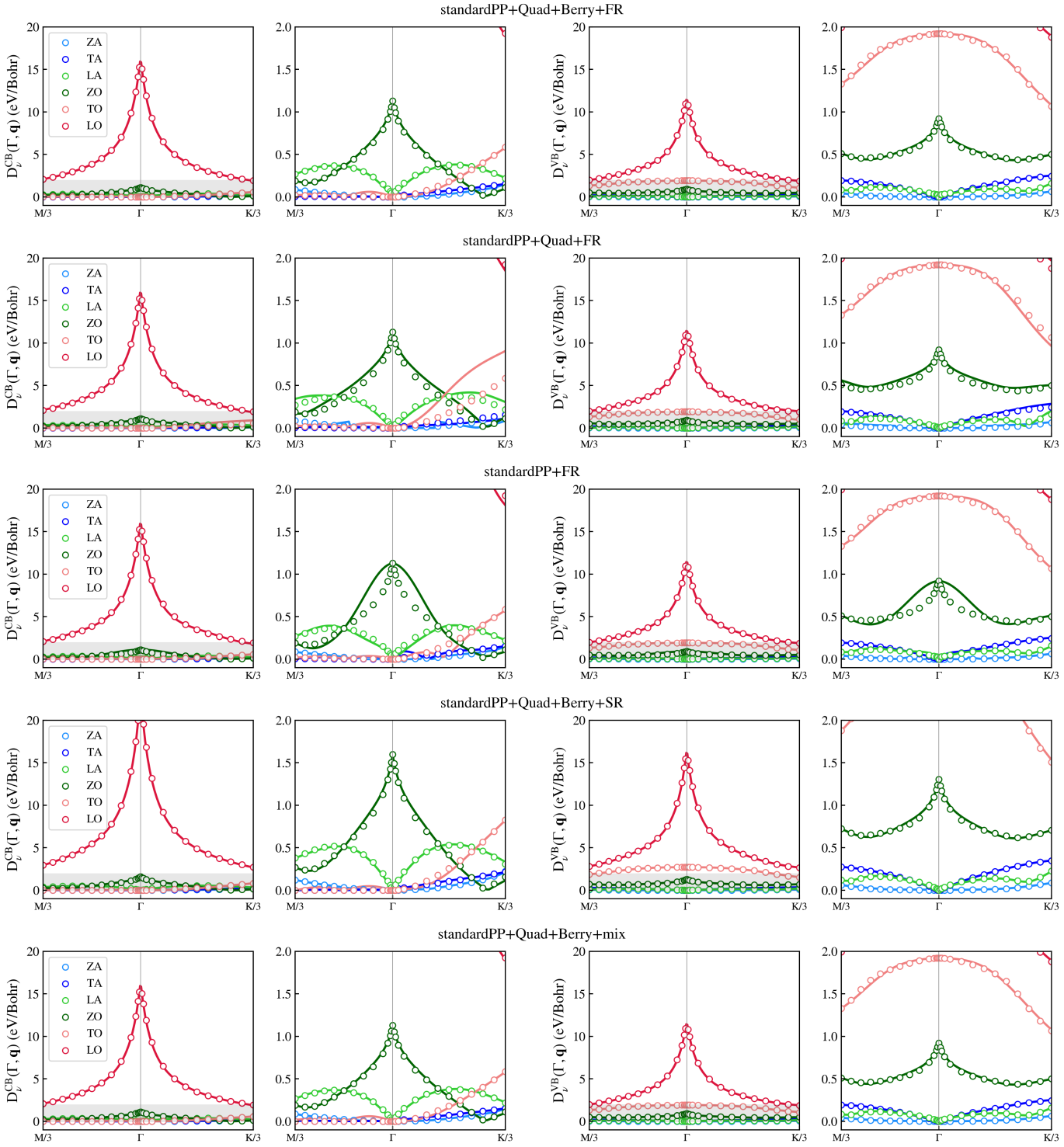


FIG. S4. Comparison between the deformation potential from the direct DFPT calculations (dots) and that from the Wannier interpolation (lines). The left two columns show the conduction bands and zoomed-in shadowed region, the right two columns show the valence bands and zoomed-in shadowed region. Note that there is a factor $\sqrt{2}$ between the SR and FR deformation potentials coming from the normalization of the spinor wavefunctions.

S4. InP

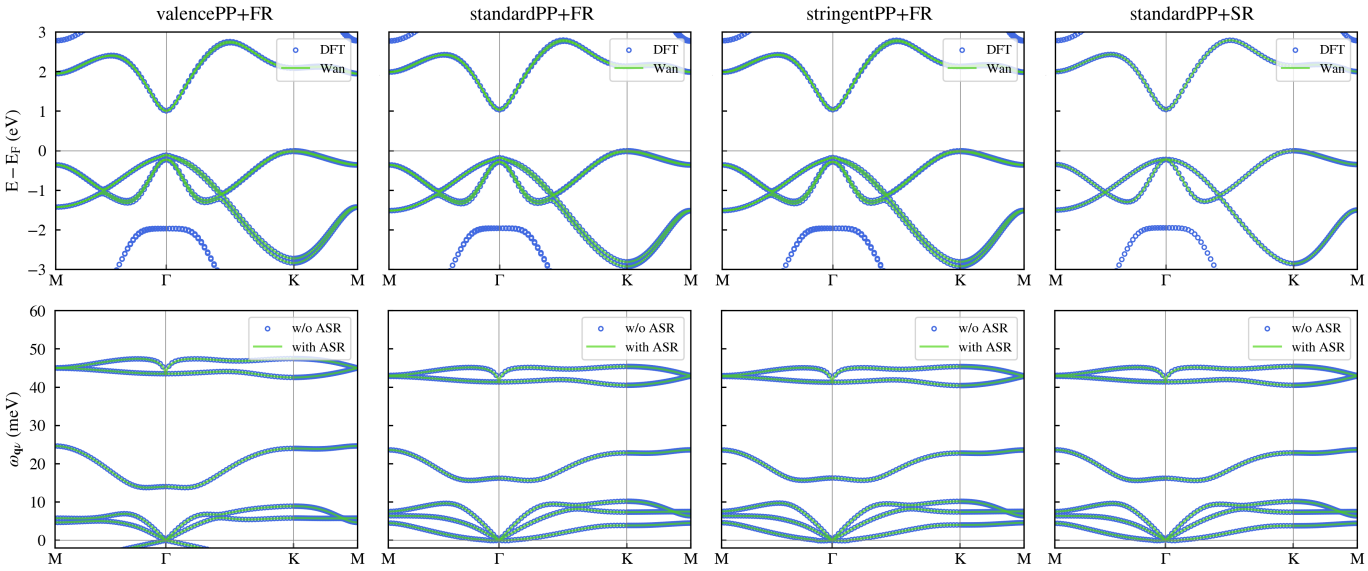


FIG. S5. Electronic bands (the first row) and phonon dispersions (the second row) calculated by different pseudopotentials. The effects of acoustic sum rule (ASR) are shown in phonon dispersions.

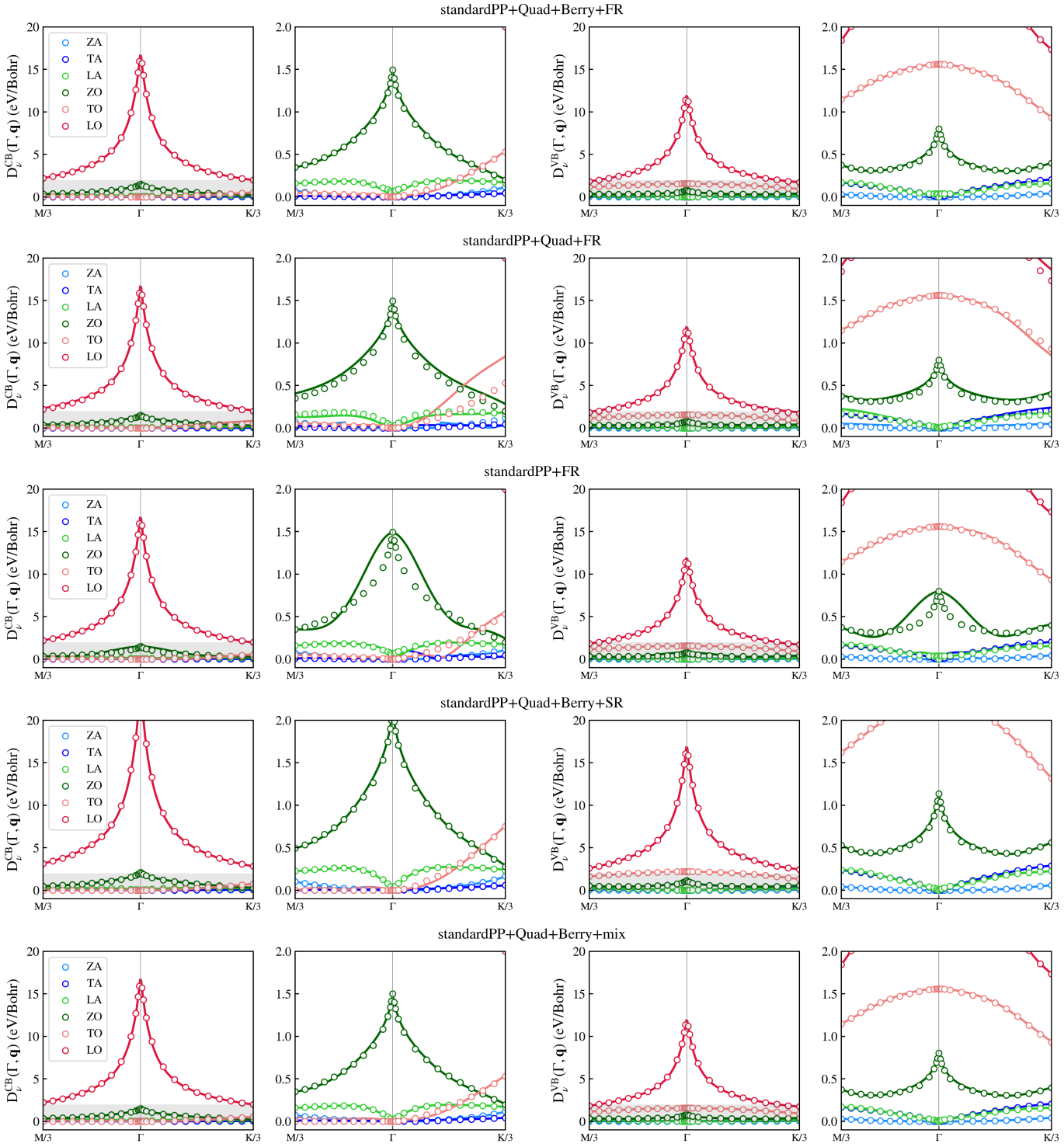


FIG. S6. Comparison between the deformation potential from the direct DFPT calculations (dots) and that from the Wannier interpolation (lines). The left two columns show the conduction bands and zoomed-in shadowed region, the right two columns show the valence bands and zoomed-in shadowed region. Note that there is a factor $\sqrt{2}$ between the SR and FR deformation potentials coming from the normalization of the spinor wavefunctions.

S5. GaAs

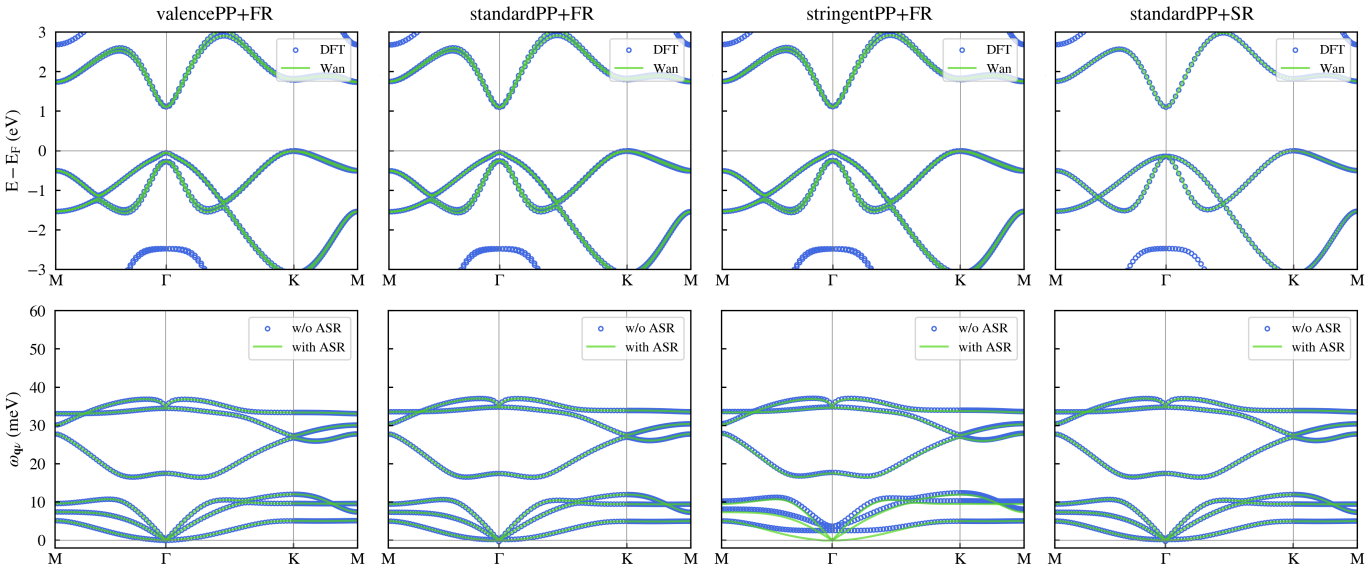


FIG. S7. Electronic bands (the first row) and phonon dispersions (the second row) calculated by different pseudopotentials. The effects of acoustic sum rule (ASR) are shown in phonon dispersions.

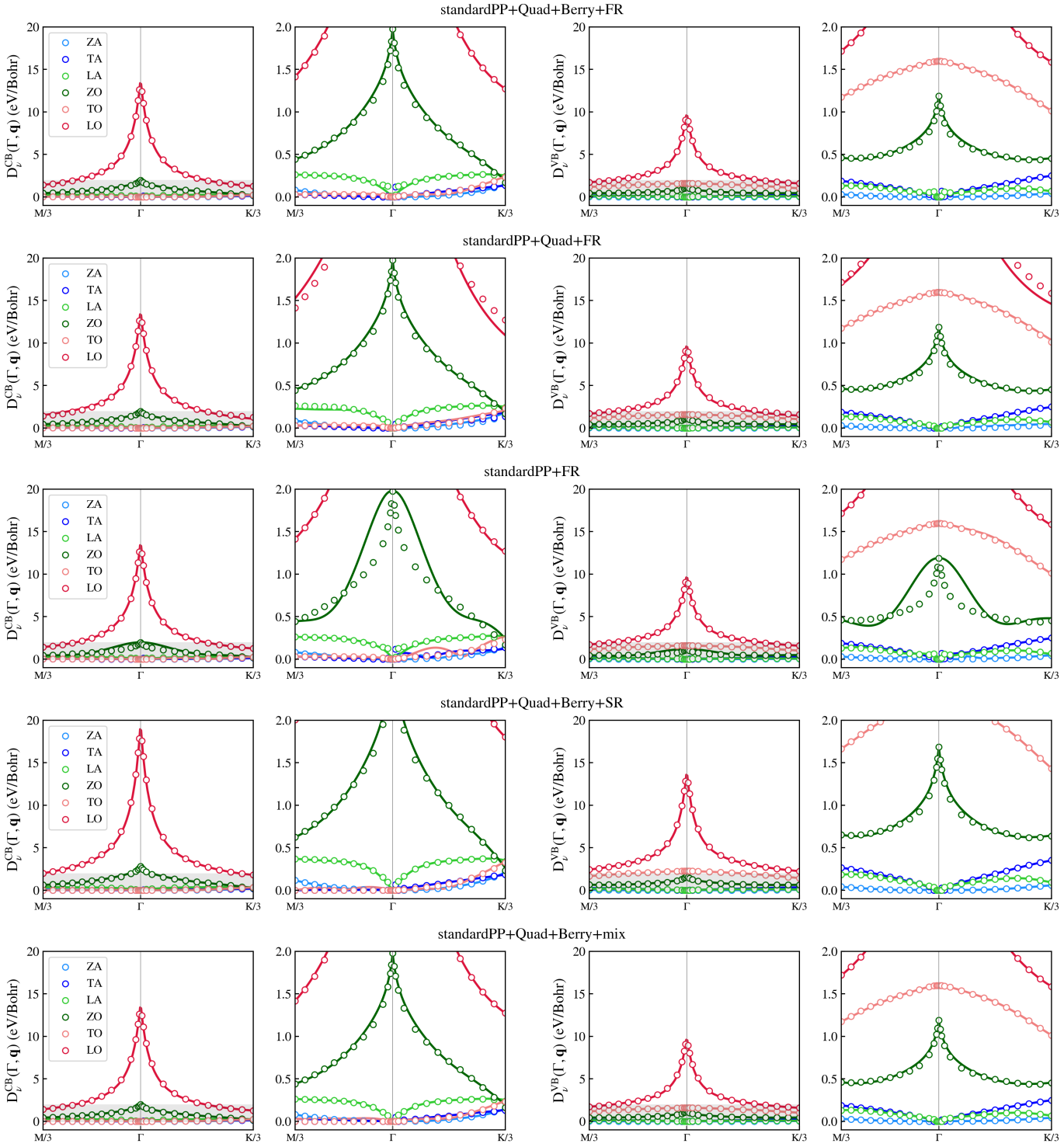


FIG. S8. Comparison between the deformation potential from the direct DFPT calculations (dots) and that from the Wannier interpolation (lines). The left two columns show the conduction bands and zoomed-in shadowed region, the right two columns show the valence bands and zoomed-in shadowed region. Note that there is a factor $\sqrt{2}$ between the SR and FR deformation potentials coming from the normalization of the spinor wavefunctions.

S6. InAs

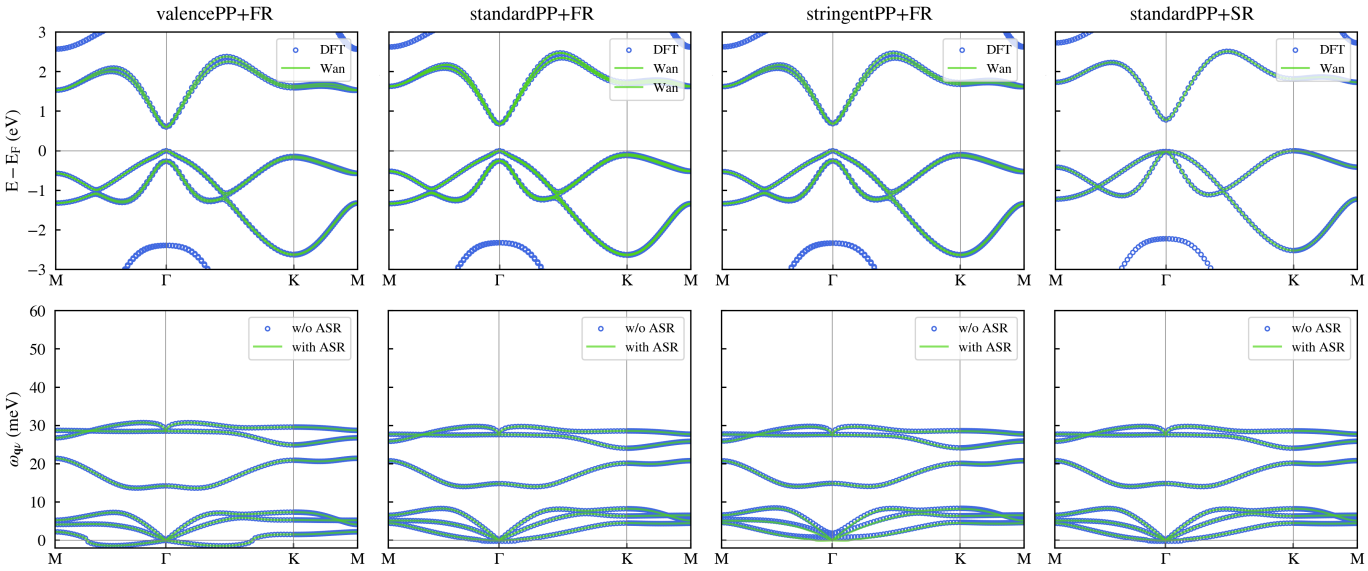


FIG. S9. Electronic bands (the first row) and phonon dispersions (the second row) calculated by different pseudopotentials. The effects of acoustic sum rule (ASR) are shown in phonon dispersions.

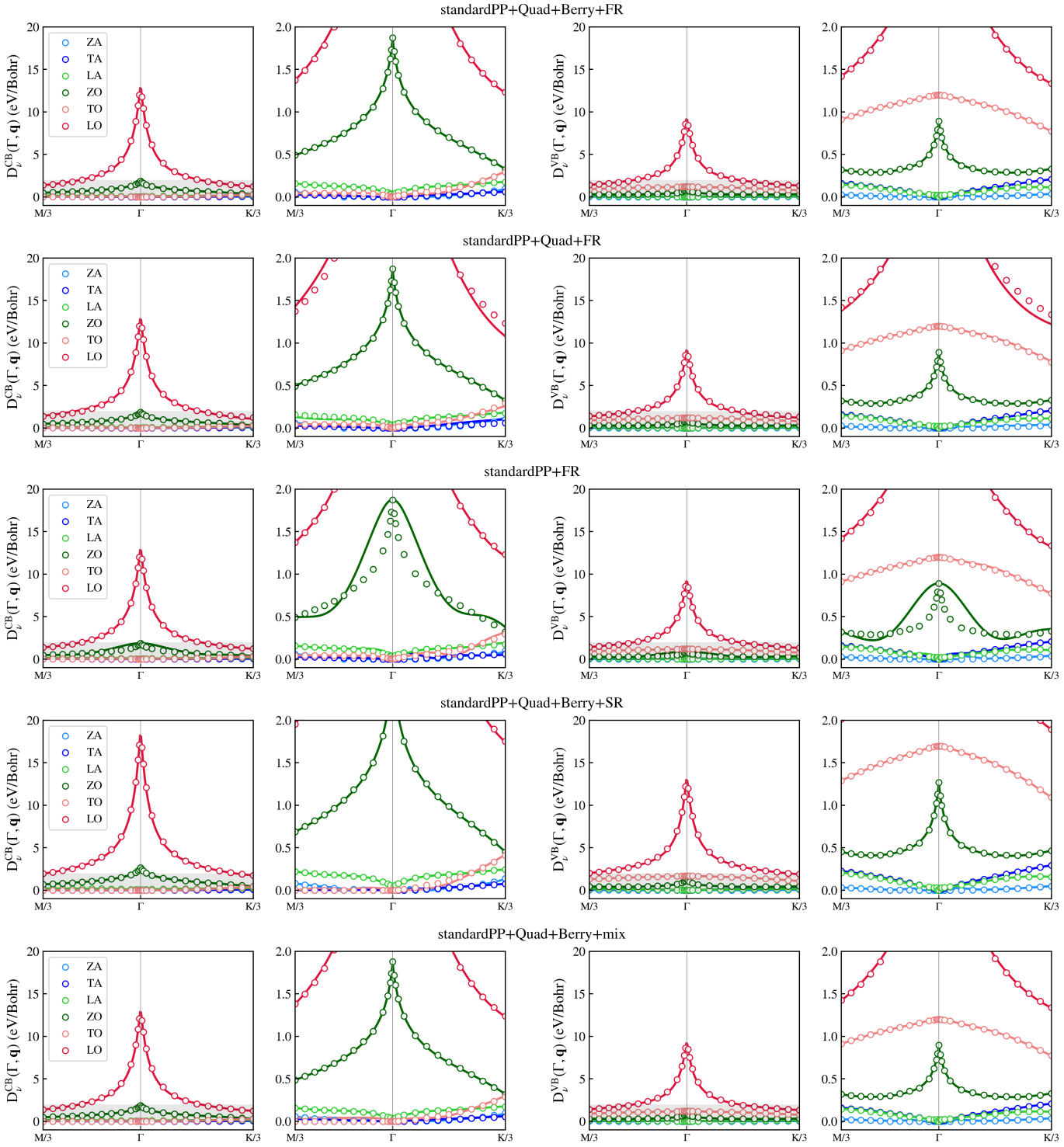


FIG. S10. Comparison between the deformation potential from the direct DFPT calculations (dots) and that from the Wannier interpolation (lines). The left two columns show the conduction bands and zoomed-in shadowed region, the right two columns show the valence bands and zoomed-in shadowed region. Note that there is a factor $\sqrt{2}$ between the SR and FR deformation potentials coming from the normalization of the spinor wavefunctions.

S7. GaSb

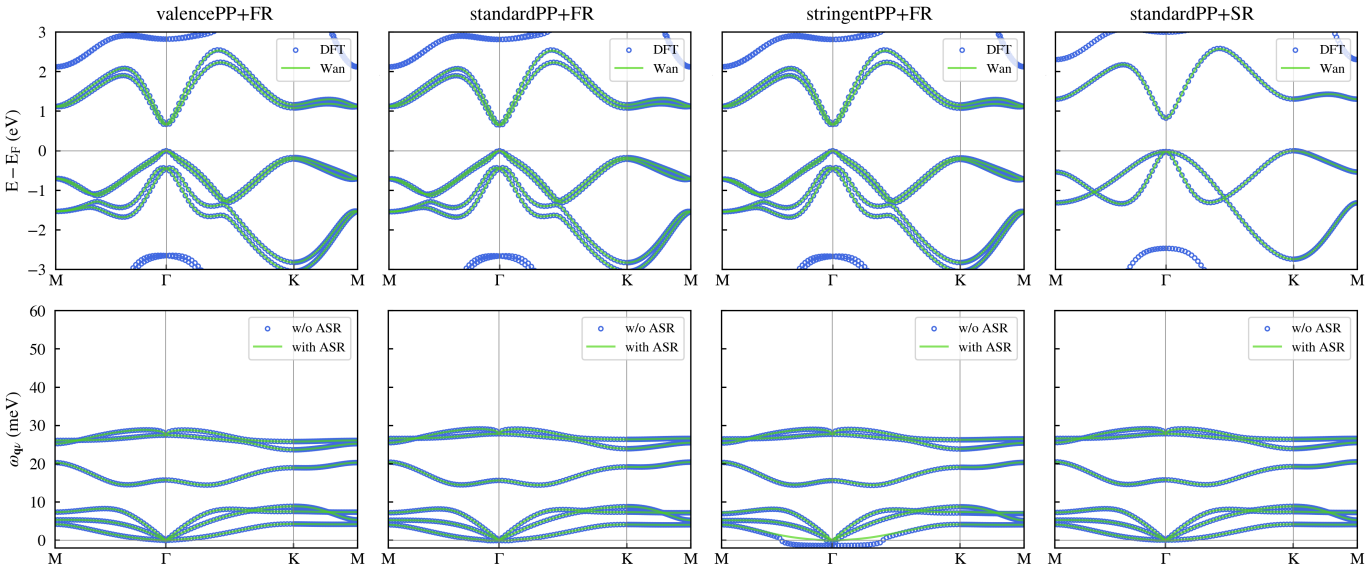


FIG. S11. Electronic bands (the first row) and phonon dispersions (the second row) calculated by different pseudopotentials. The effects of acoustic sum rule (ASR) are shown in phonon dispersions.

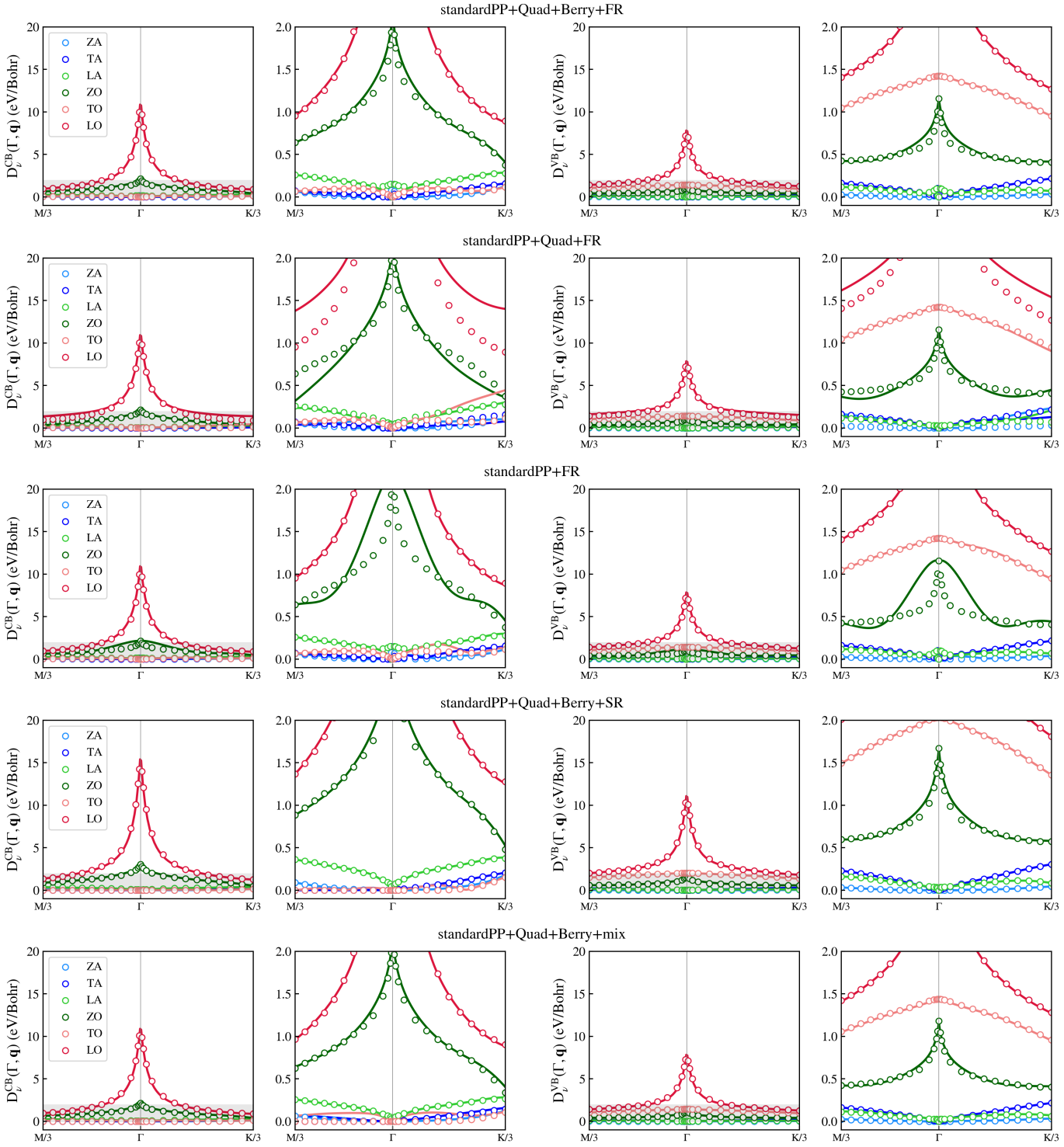


FIG. S12. Comparison between the deformation potential from the direct DFPT calculations (dots) and that from the Wannier interpolation (lines). The left two columns show the conduction bands and zoomed-in shadowed region, the right two columns show the valence bands and zoomed-in shadowed region. Note that there is a factor $\sqrt{2}$ between the SR and FR deformation potentials coming from the normalization of the spinor wavefunctions.

S8. InSb

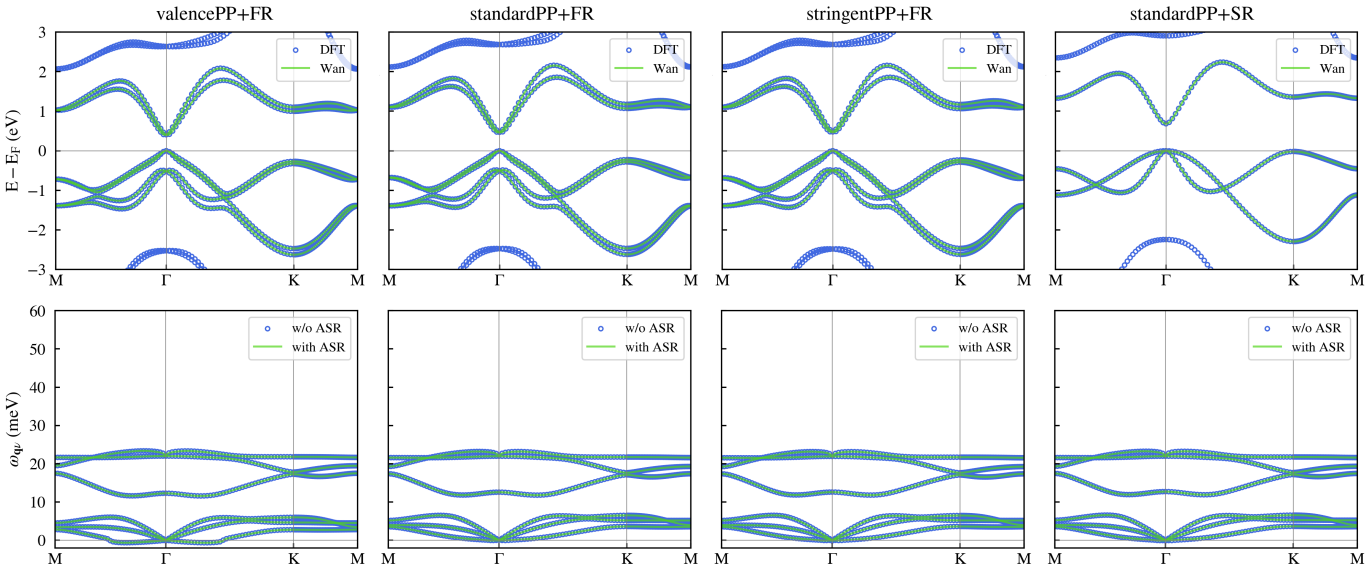


FIG. S13. Electronic bands (the first row) and phonon dispersions (the second row) calculated by different pseudopotentials. The effects of acoustic sum rule (ASR) are shown in phonon dispersions.

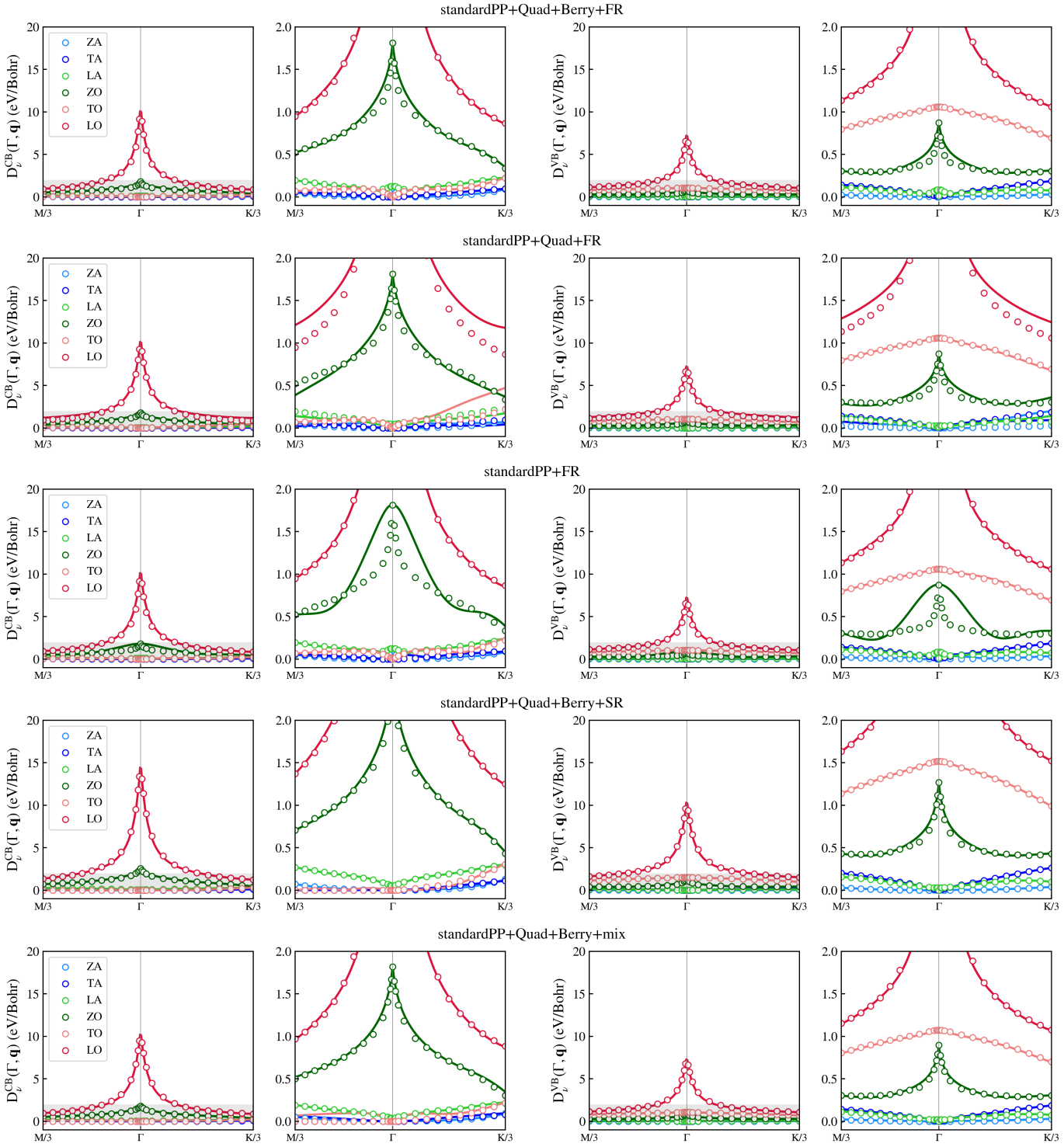


FIG. S14. Comparison between the deformation potential from the direct DFPT calculations (dots) and that from the Wannier interpolation (lines). The left two columns show the conduction bands and zoomed-in shadowed region, the right two columns show the valence bands and zoomed-in shadowed region. Note that there is a factor $\sqrt{2}$ between the SR and FR deformation potentials coming from the normalization of the spinor wavefunctions.

S9. CARRIER SCATTERING RATES, VELOCITIES, AND SPECTRAL DECOMPOSITIONS

Figure S15 presents the **k**-resolved carrier scattering rates and carrier velocities. For the electron mobility in pristine semiconductors, only intravalley scattering is allowed around Γ. For the hole mobility, the VBM positions greatly impact intervalley scattering. From GaP to InSb, the scattering at K points is decreasing, and the importance of the Γ-region increases. The large velocities around the Γ point is attributed to the small effective mass, in contrast to the situation around K points, and the velocity pattern around Γ is produced by the crystal symmetry.

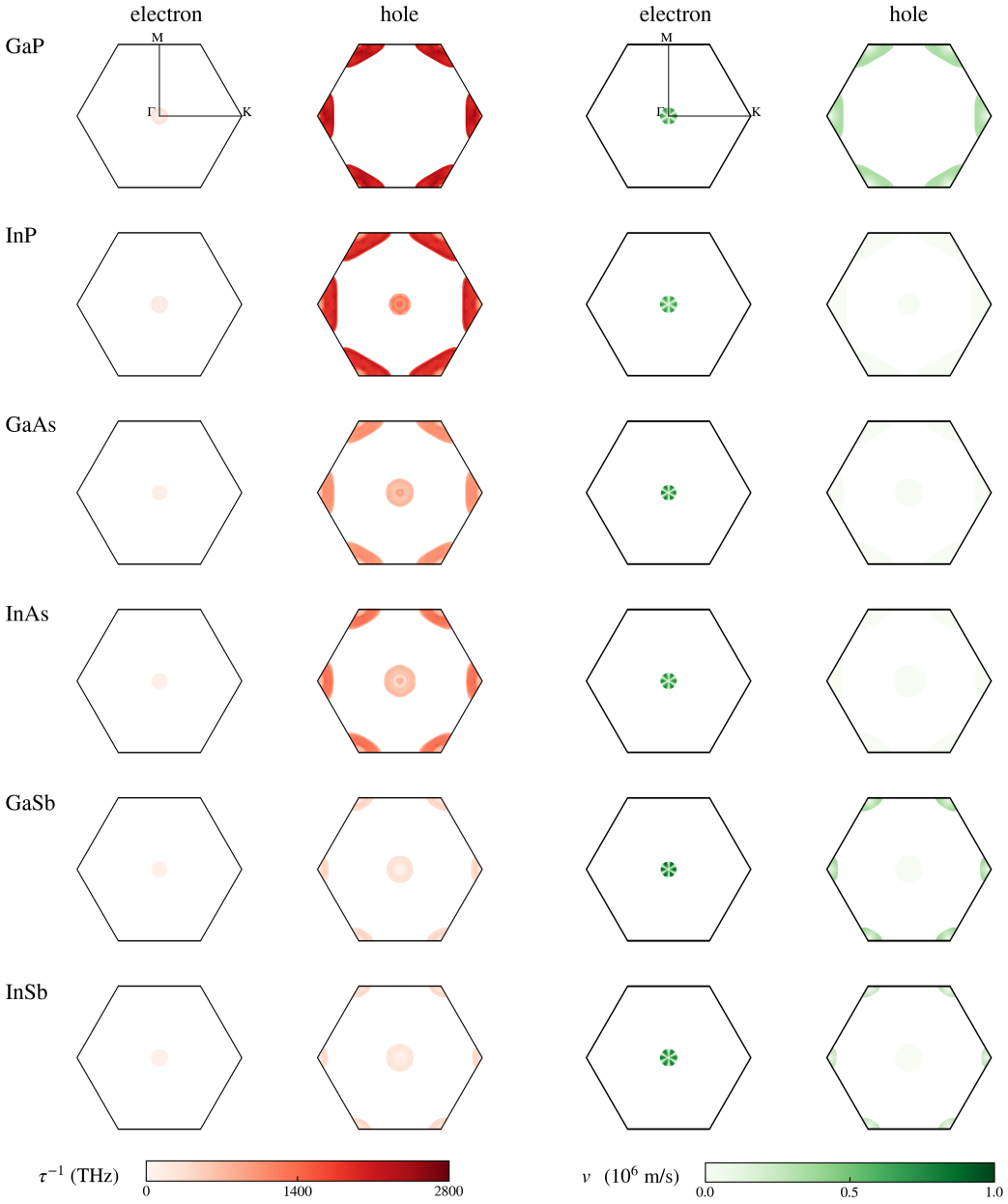


FIG. S15. **k**-resolved scattering rates τ^{-1} and velocities v integrated over all the bands in the window of 0.3 eV around E_F at 300 K.

Figure S16 presents the mode decomposition of the scattering rates for mobilities of pristine semiconductors. We focus on the band edges. For the electron mobility, scatterings mainly come from the longitudinal optical (LO) mode in all the materials. For the hole mobility, the out-of-plane acoustic (ZA) mode is dominant in phosphides and GaAs whose VBM locates at the K point, and LO mode is more prominent in InAs and antimonides whose VBM locates at Γ.

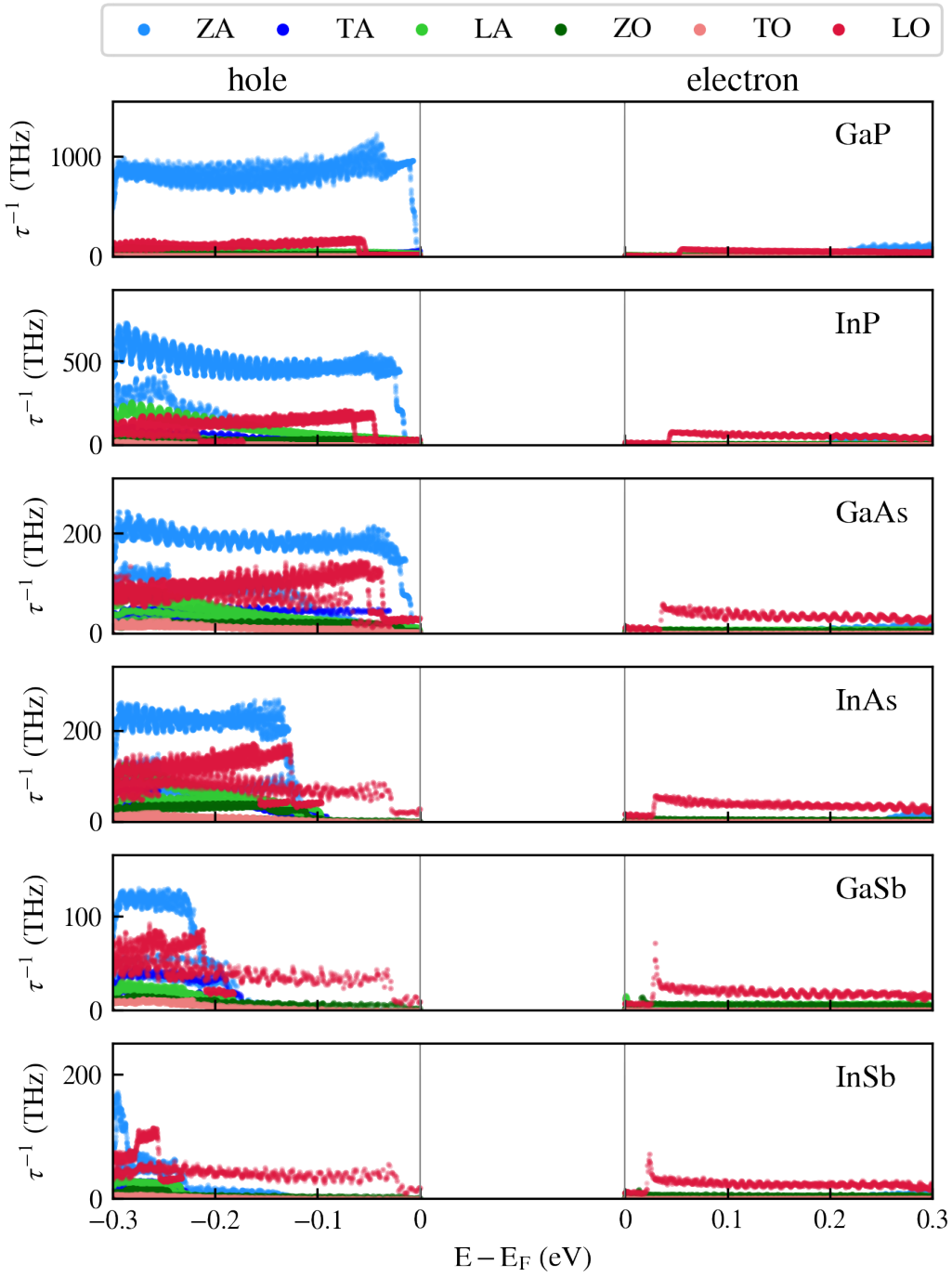


FIG. S16. Mode decomposition of scattering rates at 300 K as a function of energy from the band edge (VBM and CBM are separately set to 0) of all the III-V monolayers. The energy range covers the Fermi surface window used in transport calculations. ZA: out-of-plane acoustic; TA: transverse acoustic; LA: longitudinal acoustic; ZO: out-of-plane optical; TO: transverse optical; LO: longitudinal optical.

Figure S17 presents spectral decompositions of the electron and hole scattering rates as a function of phonon energy. Consistent with Fig. S16, high-frequency modes make major contributions to the electron mobility, as well as to the hole mobility in InAs and antimonides. Low-frequency modes are essential for the hole mobility of phosphides and GaAs.

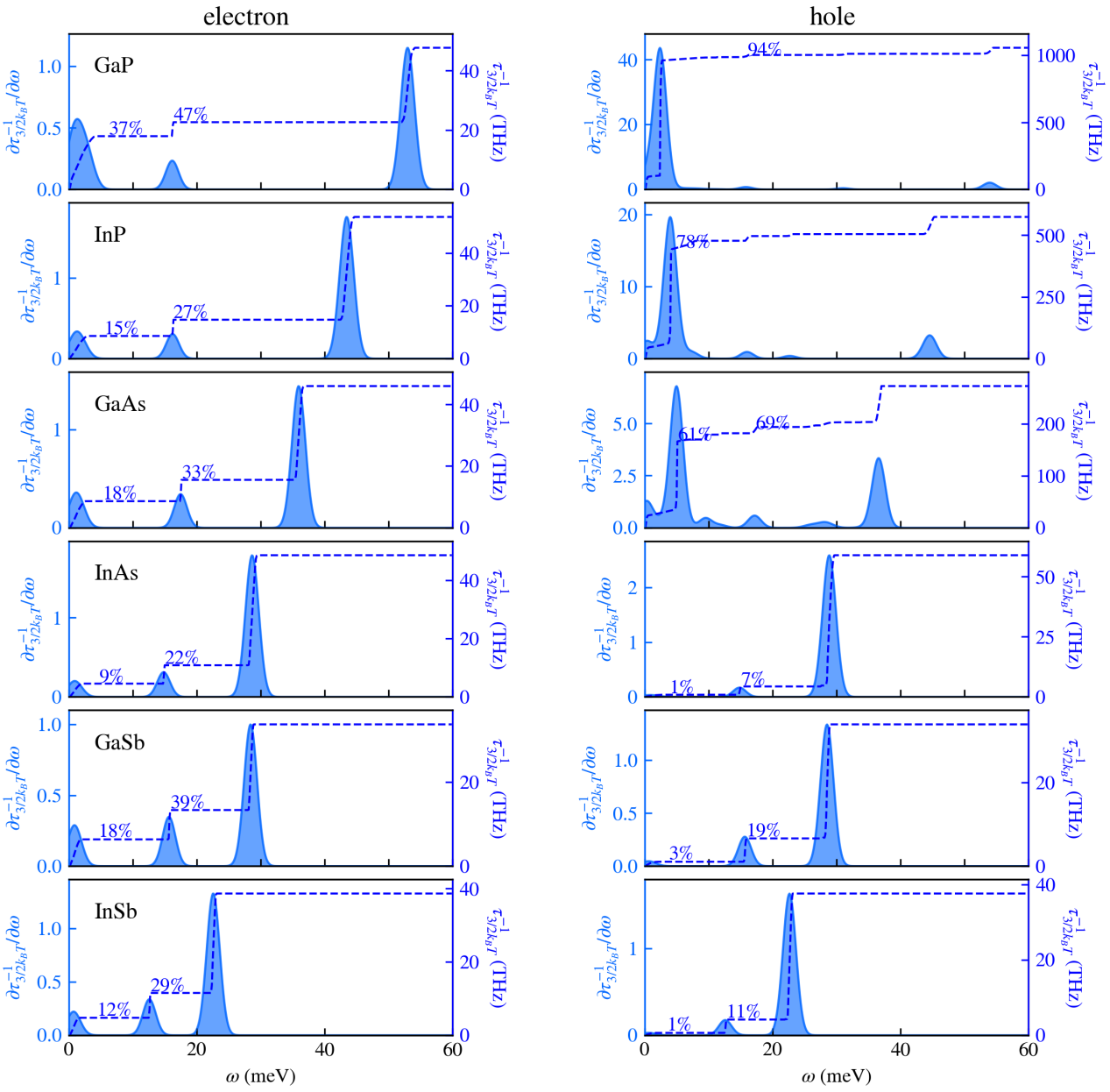


FIG. S17. Spectral decomposition of the electron (the left column) and hole (the right column) scattering rates as a function of phonon energy of all the III-V monolayers at 300 K. The rates are calculated at the energy of $3/2k_BT = 39$ meV away from the band edges. The dashed lines represent the cumulative integrals of the calculated rates, and add up to the carrier scattering rate $\tau^{-1}_{3/2k_BT}$. The percents indicate the cumulative contributions of the scattering peaks.